DOI:10.34918/85114

Maksymilian JĘDRZEJOWSKI[1], Ewa MAJCHRZAK[1,*]

Chapter 14. NUMERICAL ANALYSIS OF SKIN TUMOR FREEZING USING DUAL-PHASE LAG MODEL

14.1. Introduction

Low temperature can lead to cell necrosis. When the temperature is low enough to freeze water, ice crystals appear in extracellular spaces. Hence, a hyperosmotic extracellular environment is created, which draws water from cells, leading to the shrinkage of cells and destruction of their membranes [1]. As the temperature decreases, ice crystals appear within the cells. During thawing recrystallisation occurs, that is, ice crystals fuse and form larger crystals. When the ice melts, a hypotonic extracellular environment is created, and water flows back into cells. Their volume increases, leading to additional cell damage. Cryobiological research proved that any part of the freeze-thaw cycle may be injurious. Skin tumor (e.g. melanoma) is treated with cylindrical cryoprobe, which is applied directly to its surface (Fig. 1).

Rapid cooling is more destructive, so the cooling rate should be as high as possible [1]. Experimental data vary from 22°C / min to 50°C / min to even 220°C / min [1, 2]. However, in vitro research reports significant cell damage in a cooling ratio of as low as 1°C / min [3]. It should be noted that rapid cooling appears only near the cryoprobe, and the cooling rate is reduced as the distance from the probe increases. Taking these variances into account, the cooling rate has a low impact on injury production [1].

In cancer treatment, there is a difference between lethal and surely lethal tissue temperature. The lethal tissue temperature can be achieved in the range of –15°C to –20°C [1, 4, 5]. The cell survival rate should be minimalised; therefore, the surely

[1] Department of Computational Mechanics and Engineering, Faculty of Mechanical Engineering, Silesian University of Technology, Gliwice, Poland.
* Corresponding author: ewa.majchrzak@polsl.pl.

lethal tissue temperature can be established below –40°C [1, 4, 5]. In some experiments, the lethal dose is defined as low as –60°C with the requirement of repetitive freeze-thaw cycles [6]. However, the temperature –40°C nowadays is defined as a lethal dose in a variety of research, connecting this temperature with the physics of water (the crystal growth is highest in the range from 0°C to –40°C [1]).

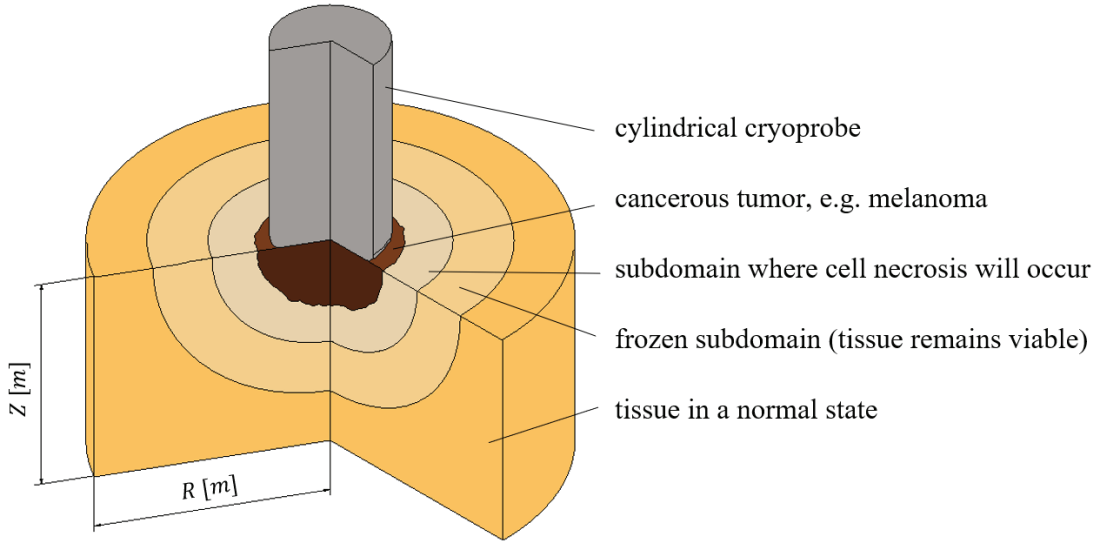

Fig. 1. Considered domain
Rys. 1. Rozważany obszar

The thawing rate is a key destructive factor. Cell damage increases greatly with prolonged thawing and the thawing rate should be as low as 1°C / min [7]. Rapid thawing increases cell survival ratio very highly. In fact, slow thawing is more important in cell destruction than rapid cooling [1, 7, 8].

Repetition of the freeze-thaw cycle increases previously frozen volume and intensifies cell necrosis. For example, in the treatment of facial basal cell carcinomas, the cure rate for the double freeze-thaw cycle is 95.3% compared to only 79.4% for the single freeze-thaw cycle [9]. The effect of repeated freeze-thaw cycles has a greater impact on cure rates when the freeze temperature is relatively warm, e.g. –20°C.

Mathematical modelling methods are extremely helpful in planning cryosurgical procedures. They allow for the analysis of many variants of freezing with different cooling rates, number of freeze-thaw cycles, and different durations of the process. In this paper, the freezing process is described by the dual-phase lag equation supplemented with appropriate boundary and initial conditions. The problem is solved

using the finite difference method both in the explicit and implicit schemes. Using an in-house computer program, the temperature distribution in the domain analysed is calculated, the subdomain of the frozen region is determined, and the effectiveness of freezing the tumor is estimated.

14.2. Mathematical model

In 1995 Tzou [10] proposed the introduction of two time lags in Fourier law, representing a macroscopic lag (delayed response) between the temperature gradient and the heat flux as a result of microstructural effects, governing the following formula

$$\boldsymbol{q}(\mathbf{x}, t + \tau_q) = -\lambda \nabla T(\mathbf{x}, t + \tau_T) \tag{1}$$

where $\boldsymbol{q}$ is the heat flux vector, $\mathbf{x} = \{r, z\}$ denotes geometrical coordinates, t is the time, λ is thermal conductivity, τ_q and τ_T are the phase lags (called relaxation and thermalization time respectively).

The following first-order (linear) approximation can be obtained with the use of Taylor series expansions

$$\boldsymbol{q}(\mathbf{x}, t) + \tau_q \frac{\partial \boldsymbol{q}(\mathbf{x}, t)}{\partial t} \cong -\lambda \left[\nabla T(\mathbf{x}, t) + \tau_T \frac{\partial \nabla T(\mathbf{x}, t)}{\partial t} \right] \tag{2}$$

Both phase lags are assumed to be small, so nonlinear orders are negligible [10].

Introducing formula (2) to the well known macroscopic energy equation one obtains [10, 11]

$$c \left[\frac{\partial T(\mathbf{x}, t)}{\partial t} + \tau_q \frac{\partial^2 T(\mathbf{x}, t)}{\partial t^2} \right] = \nabla [\lambda \nabla T(\mathbf{x}, t)] + \tau_T \nabla \left[\lambda \frac{\partial \nabla T(\mathbf{x}, t)}{\partial t} \right] \tag{3}$$

where c is the volumetric specific heat.

In biological tissue, internal heat sources should also be considered, which gives the following dual-phase lag equation (DPLE) [11]

$$c\left[\frac{\partial T(\mathbf{x},t)}{\partial t}+\tau_q\frac{\partial^2 T(\mathbf{x},t)}{\partial t^2}\right] = \nabla[\lambda\nabla T(\mathbf{x},t)]+\tau_T\nabla\left[\lambda\frac{\partial\nabla T(\mathbf{x},t)}{\partial t}\right]+Q(\mathbf{x},t)+\tau_q\frac{\partial Q(\mathbf{x},t)}{\partial t}+Q_F(\mathbf{x},t) + \tau_q\frac{\partial Q_F(\mathbf{x},t)}{\partial t} \tag{4}$$

Internal heat source $Q(\mathbf{x},t)$, related to blood perfusion and metabolism, is defined as the following sum

$$Q(\mathbf{x},t)=wc_b[T_a-T(\mathbf{x},t)]+Q_{met}(T) \tag{5}$$

where w is the blood perfusion rate, c_b is the specific heat of the blood, T_a is the arterial blood temperature, Q_{met} is the metabolic heat source.

The internal volumetric heat source $Q_F(\mathbf{x},t)$, related to the phase change, is defined as

$$Q_F(\mathbf{x},t)=L\frac{\partial S(\mathbf{x},t)}{\partial t}=L\frac{\mathrm{d}S(T)}{\mathrm{d}T}\frac{\partial T(\mathbf{x},t)}{\partial t} \tag{6}$$

where L is the volumetric latent heat of freezing and $S(\mathbf{x},t)$ is the frozen state fraction.

After determining the derivatives and some transformations, one can obtain

$$Q(\mathbf{x},t)+\tau_q\frac{\partial Q(\mathbf{x},t)}{\partial t}+Q_F(\mathbf{x},t)+\tau_q\frac{\partial Q_F(\mathbf{x},t)}{\partial t} = \tau_q\left[\frac{\mathrm{d}w(T)}{\mathrm{d}T}c_b(T_a-T)-w(T)c_b+\frac{\mathrm{d}Q_{met}(T)}{\mathrm{d}T}\right]\frac{\partial T}{\partial t}+w(T)c_b(T_a-T) + Q_{met}(T)+L\frac{\mathrm{d}S(T)}{\mathrm{d}T}\frac{\partial T}{\partial t}+\tau_q L\left[\frac{\mathrm{d}^2S(T)}{\mathrm{d}T^2}\left(\frac{\partial T}{\partial t}\right)^2+\frac{\mathrm{d}S(T)}{\mathrm{d}T}\frac{\partial^2 T}{\partial t^2}\right] \tag{7}$$

and by denoting the derivative of the blood perfusion rate and the derivative of the metabolic heat as

$$v(T)=\frac{\mathrm{d}w(T)}{\mathrm{d}T},\qquad P_{met}(T)=\frac{\mathrm{d}Q_{met}(T)}{\mathrm{d}T} \tag{8}$$

the dual-phase lag equation (4) can be written as follows

$$\left[C(T)+\tau_q\{w(T)c_b-v(T)c_b(T_a-T)-P_{met}(T)\}\right]\frac{\partial T}{\partial t}+\tau_q C(T)\frac{\partial^2 T}{\partial t^2}+\tau_q\frac{\mathrm{d}C(T)}{\mathrm{d}T}\left(\frac{\partial T}{\partial t}\right)^2 = \nabla(\lambda(T)\nabla\mathrm{T})+\tau_T\nabla\left[\lambda(T)\nabla\left(\frac{\partial T}{\partial t}\right)\right]+w(T)c_b(T_a-T)+Q_{met}(T) \tag{9}$$

where C is a substitute thermal capacity of the intermediate region [11]

$$C(T) = c(T) - L\frac{\mathrm{d}S(T)}{\mathrm{d}T} \tag{10}$$

In this paper, the following functions have been assumed that describe the dependence of the blood perfusion rate and the metabolic heat source on the temperature

$$w(T) = \begin{cases} w_0 & T > T_1 \\ w_0 \dfrac{T - T_2}{T_1 - T_2} & T_2 \le T \le T_1 \\ 0 & T < T_2 \end{cases} \tag{11}$$

$$Q_{met}(T) = \begin{cases} Q_{met0} & T > T_1 \\ Q_{met0} \dfrac{T - T_2}{T_1 - T_2} & T_2 \le T \le T_1 \\ 0 & T < T_2 \end{cases} \tag{12}$$

where T_1 is the beginning temperature of freezing and T_2 is the ending temperature of freezing. If part of the tissue is frozen and thawed, then the blood perfusion rate and the metabolic heat source are permanently equal to zero due to the destruction of blood vessels in that region [11]. The derivatives of these two parameters are given as follows

$$v(T) = \begin{cases} 0 & T > T_1 \\ w_0 \dfrac{1}{T_1 - T_2} & T_2 \le T \le T_1 \\ 0 & T < T_2 \end{cases} \tag{13}$$

$$P_{met}(T) = \begin{cases} 0 & T > T_1 \\ Q_{met0} \dfrac{1}{T_1 - T_2} & T_2 \le T \le T_1 \\ 0 & T < T_2 \end{cases} \tag{14}$$

where w_0 and Q_{met0} are the values determined for the tissue in its natural state.

In the temperature range $[T_2, T_1]$ a linear function was assumed to describe the frozen state fraction

$$S(T) = \frac{T_1 - T}{T_1 - T_2} \tag{15}$$

Therefore, the substitute thermal capacity can be written as

$$C = \begin{cases} c_N & T > T_1 \\ c_P + \dfrac{L}{T_1 - T_2} & T_2 \le T \le T_1 \\ c_F & T < T_2 \end{cases} \tag{16}$$

where c_N, c_P, and c_F denote the thermal capacity of tissue in its natural, intermediate, and frozen state, respectively. Substitute thermal capacity (eq. (16)) in this article is a step function, thus eq. (9) can be written in the following form

$$\begin{aligned}\left[C(T)+\tau_q\{w(T)c_b-v(T)c_b(T_a-T)-P_{met}(T)\}\right]\frac{\partial T}{\partial t}+\tau_q C(T)\frac{\partial^2 T}{\partial t^2}\\ =\nabla(\lambda(T)\nabla\mathrm{T})+\tau_T\nabla\left[\lambda(T)\nabla\left(\frac{\partial T}{\partial t}\right)\right]+w(T)c_b(T_a-T)+Q_{met}(T)\end{aligned} \tag{17}$$

Also, the thermal conductivity is a step function given as

$$\lambda=\begin{cases}\lambda_N & T>T_1\\ \lambda_P & T_2\le T\le T_1\\ \lambda_F & T<T_2\end{cases} \tag{18}$$

where λ_N, λ_P, λ_F denote the thermal conductivity of the tissue, in its natural, intermediate and frozen state, respectively.

On the contact surface between the tip of the cryoprobe and the skin tissue, the Dirichlet condition is assumed

$$T=T_D(t) \tag{19}$$

and on the other surfaces the adiabatic boundary condition is assumed

$$-\lambda\left[\boldsymbol{n}\cdot\nabla T(\mathbf{x},t)+\tau_T\frac{\partial[\boldsymbol{n}\cdot\nabla T(\mathbf{x},t)]}{\partial t}\right]=0 \tag{20}$$

where $\boldsymbol{n}\cdot\nabla T(\mathbf{x},t)$ is the normal derivative.

The initial conditions are given as follows

$$t=0:\quad T=T_p,\quad \left.\frac{\partial T}{\partial t}\right|_{t=0}=u \tag{21}$$

where T_p is the initial temperature and u is the initial cooling rate.

As mentioned earlier, the phase lags τ_q and τ_T are small constant values [10]. DPLM can be reduced to thermal wave equations (hyperbolic model) for τ_T = 0 s [10, 12]. The classic Fourier equation (parabolic model) can be obtained by substituting τ_q = τ_T = 0 s. It should be noted that the dual-phase effect in biological tissue is important even for $\tau_q \approx \tau_T$ [13].

14.3. Numerical model

In a cylindrical coordinate system eq. (17) can be written as

$$\begin{aligned}\left[C(T)+\tau_q\{w(T)c_b-v(T)c_b(T_a-T)-P_{met}(T)\}\right]\frac{\partial T}{\partial t}+\tau_q C(T)\frac{\partial^2 T}{\partial t^2}\\ =\frac{1}{r}\lambda(T)\left[\frac{\partial T}{\partial r}+\tau_T\frac{\partial}{\partial r}\left(\frac{\partial T}{\partial t}\right)\right]+\lambda(T)\left[\frac{\partial^2 T}{\partial r^2}+\tau_T\frac{\partial^2}{\partial r^2}\left(\frac{\partial T}{\partial t}\right)\right]\\ +\lambda(T)\left[\frac{\partial^2 T}{\partial z^2}+\tau_T\frac{\partial^2}{\partial z^2}\left(\frac{\partial T}{\partial t}\right)\right]+w(T)c_b(T_a-T)+Q_{met}(T)\end{aligned} \tag{22}$$

Numerical computations are carried out using the finite difference method (FDM) [14]. The time grid with the constant time step Δt is introduced. The quadratic mesh with the constant grid step h is applied.

Using the explicit FDM scheme eq. (22) can be written as

$$T_{i,j}^{f}=\frac{M_{i,j}^{f-1}}{K_{i,j}^{f-1}}T_{i,j}^{f-1}+\frac{P_{i,j}^{f-1}}{K_{i,j}^{f-1}}T_{i,j+1}^{f-1}+\frac{R_{i,j}^{f-1}}{K_{i,j}^{f-1}}T_{i,j-1}^{f-1}+\frac{S_{i,j}^{f-1}}{K_{i,j}^{f-1}}\left(T_{i-1,j}^{f-1}+T_{i+1,j}^{f-1}\right)+\frac{W_{i,j}^{f-1}}{K_{i,j}^{f-1}} \tag{23}$$

where

$$\begin{aligned}K_{i,j}^{f-1}&=\frac{\left[C_{i,j}^{f-1}+\tau_q\left\{w_{i,j}^{f-1}c_b-v_{i,j}^{f-1}c_b\left(T_a-T_{i,j}^{f-1}\right)-{P_{met}}_{i,j}^{f-1}\right\}\right]\Delta t+\tau_q C_{i,j}^{f-1}}{(\Delta t)^2}\\ M_{i,j}^{f-1}&=\frac{\left[C_{i,j}^{f-1}+\tau_q\left\{w_{i,j}^{f-1}c_b-v_{i,j}^{f-1}c_b\left(T_a-T_{i,j}^{f-1}\right)-{P_{met}}_{i,j}^{f-1}\right\}\right]\Delta t+2\tau_q C_{i,j}^{f-1}}{(\Delta t)^2}\\ &\quad-4\frac{\lambda_{i,j}^{f-1}(\Delta t+\tau_T)}{h^2\Delta t}-w_{i,j}^{f-1}c_b\\ P_{i,j}^{f-1}&=\frac{\lambda_{i,j}^{f-1}(\Delta t+\tau_T)}{h^2\Delta t}+\frac{\lambda_{i,j}^{f-1}(\Delta t+\tau_T)}{2hr_{i,j}\Delta t}\\ R_{i,j}^{f-1}&=\frac{\lambda_{i,j}^{f-1}(\Delta t+\tau_T)}{h^2\Delta t}-\frac{\lambda_{i,j}^{f-1}(\Delta t+\tau_T)}{2hr_{i,j}\Delta t}\\ S_{i,j}^{f-1}&=\frac{\lambda_{i,j}^{f-1}(\Delta t+\tau_T)}{h^2\Delta t}\\ W_{i,j}^{f-1}&=\left[4\frac{\lambda_{i,j}^{f-1}\tau_T}{h^2\Delta t}-\frac{\tau_q C_{i,j}^{f-1}}{(\Delta t)^2}\right]T_{i,j}^{f-2}+\left[-\frac{\lambda_{i,j}^{f-1}\tau_T}{2hr_{i,j}\Delta t}-\frac{\lambda_{i,j}^{f-1}\tau_T}{h^2\Delta t}\right]T_{i,j+1}^{f-2}\\ &\quad+\left[\frac{\lambda_{i,j}^{f-1}\tau_T}{2hr_{i,j}\Delta t}-\frac{\lambda_{i,j}^{f-1}\tau_T}{h^2\Delta t}\right]T_{i,j-1}^{f-2}+\left[-\frac{\lambda_{i,j}^{f-1}\tau_T}{h^2\Delta t}\right]\left(T_{i-1,j}^{f-2}+T_{i+1,j}^{f-2}\right)+w_{i,j}^{f-1}c_bT_a\\ &\quad+{Q_{met}}_{i,j}^{f-1}\end{aligned} \tag{24}$$

and using the FDM implicit scheme eq. (22) can be written as

$$T_{i,j}^{f} = \frac{B_{i,j}^{f-1}}{A_{i,j}^{f-1}} T_{i,j-1}^{f} + \frac{D_{i,j}^{f-1}}{A_{i,j}^{f-1}} T_{i,j+1}^{f} + \frac{F_{i,j}^{f-1}}{A_{i,j}^{f-1}} \left(T_{i-1,j}^{f} + T_{i+1,j}^{f} \right) + \frac{G_{i,j}^{f-1}}{A_{i,j}^{f-1}} \tag{25}$$

where

$$\begin{aligned}
A_{i,j}^{f-1} &= \frac{\left[C_{i,j}^{f-1} + \tau_q \left\{ w_{i,j}^{f-1} c_b - v_{i,j}^{f-1} c_b \left(T_a - T_{i,j}^{f-1} \right) - {P_{met}}_{i,j}^{f-1} \right\} \right] \Delta t + C_{i,j}^{f-1} \tau_q}{(\Delta t)^2} + w_{i,j}^{f-1} c_b \\
&\quad + 4 \frac{\lambda_{i,j}^{f-1} (\Delta t + \tau_T)}{h^2 \Delta t} \\
B_{i,j}^{f-1} &= \frac{\lambda_{i,j}^{f-1} (\Delta t + \tau_T)}{h^2 \Delta t} - \frac{\lambda_{i,j}^{f-1} (\Delta t + \tau_T)}{2 h r_{i,j} \Delta t} \\
D_{i,j}^{f-1} &= \frac{\lambda_{i,j}^{f-1} (\Delta t + \tau_T)}{h^2 \Delta t} + \frac{\lambda_{i,j}^{f-1} (\Delta t + \tau_T)}{2 h r_{i,j} \Delta t} \\
F_{i,j}^{f-1} &= \frac{\lambda_{i,j}^{f-1} (\Delta t + \tau_T)}{h^2 \Delta t} \\
G_{i,j}^{f-1} &= \left[\frac{\left[C_{i,j}^{f-1} + \tau_q \left\{ w_{i,j}^{f-1} c_b - v_{i,j}^{f-1} c_b \left(T_a - T_{i,j}^{f-1} \right) - {P_{met}}_{i,j}^{f-1} \right\} \right] \Delta t + 2 C_{i,j}^{f-1} \tau_q}{(\Delta t)^2} \right] T_{i,j}^{f-1} \\
&\quad - \frac{\lambda_{i,j}^{f-1} \tau_T}{h^2 \Delta t} \left(T_{i,j-1}^{f-1} + T_{i,j+1}^{f-1} + T_{i-1,j}^{f-1} + T_{i+1,j}^{f-1} - 4 T_{i,j}^{f-1} \right) \\
&\quad - \frac{\lambda_{i,j}^{f-1} \tau_T}{2 h r_{i,j} \Delta t} \left(T_{i,j+1}^{f-1} - T_{i,j-1}^{f-1} \right) - \frac{C_{i,j}^{f-1} \tau_q}{(\Delta t)^2} T_{i,j}^{f-2} + w_{i,j}^{f-1} c_b T_a + {Q_{met}}_{i,j}^{f-1}
\end{aligned} \tag{26}$$

The system of linear equations in the implicit scheme is solved iteratively.

Both schemes presented must be supplemented by boundary conditions. In an explicit scheme, stability condition must be fulfilled [15]. The implicit scheme of the finite difference method for the DPLE is always stable [16].

14.4. Results of computations

The cylindrical tissue domain of dimensions R = 0.04 m, Z = 0.04 m at initial temperature T_p = 37°C is considered. The tip of the cryoprobe of diameter D = 0.025 m is subjected to the skin. Thermophysical parameters are as follows: thermal conductivities λ_N = 0.52 W/(m K), λ_P = 1.26 W/(m K), λ_F = 2 W/(m K), volumetric specific heats c_N = 3.6 MJ/(m^3 K), c_P = 2.78 MJ/(m^3 K), c_F = 1.93 MJ/(m^3 K), blood

perfusion rate in natural state w_0 = 0.5 kg/(m^3 s), metabolic heat source in natural state Q_{met0} = 245 W/m^3, specific heat of blood c_b = 3770 J/(kg K), arterial blood temperature T_a = 37°C, volumetric latent heat of freezing L = 330 MJ/m^3, intermediate zone [–8°C, –1°C], that is T_2 = –8°C and T_1 = –1°C [11].

Stage III malignant melanoma is considered. The diameter of tumor infiltration is 30 mm (approximately 20 mm of the main tumor accompanied by satellite tumors) and its depth is 5 mm [17, 18]. The initial cryoprobe temperature is 37°C. The final temperature of the cryoprobe is –160°C and four freeze-thaw cycles are considered [19]. The cooling rate is set at 120°C / min and the thawing rate is set at 5°C / min. After the cooling stage, the constant temperature is maintained for 5 min. The dependence of the cryoprobe temperature on time is shown in Fig. 2.

Four cases of phase lags values were considered. Case 1 in which τ_q = 0 s and τ_T = 0 s represents the Pennes model. Case 2 in which τ_q = 0.48 s and τ_T = 0.48 s is based on the results published in [13]. Case 3 in which τ_q = 3 s and τ_T = 0.1 s is discussed in more detail in [11, 12]. Case 4 in which τ_q = 15 s and τ_T = 10 s is taken from [20].

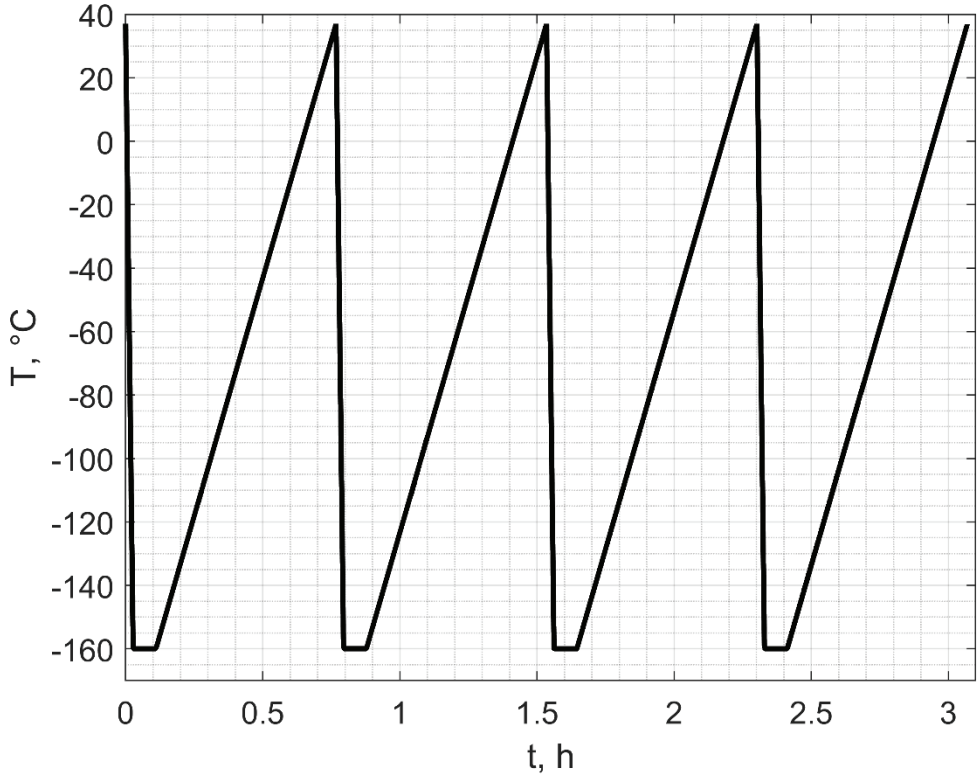

Fig. 2. Temperature of the cryoprobe
Rys. 2. Temperatura kriosondy

The influence of delay times on the obtained results was tested on the first freezing (Fig. 3). Explicit (solid line) and implicit (dashed line) schemes were compared. The results were obtained for: the number of nodes 51 × 51, grid step h = 0.0008 m, time step Δt = 0.05 s. The results are similar for both schemes for all cases. The differences between the Pennes model and the DPLM are most notable near the axis of symmetry and near the cryoprobe.

The next calculations were performed using the implicit scheme of the finite difference method under the assumption that the time step is equal to Δt = 1 s and phase lags are equal to τ_q = 3 s, τ_T = 0.1 s, respectively (case 3). As shown in Fig. 4, this time step gives results similar to those for Δt = 0.1 s and Δt = 0.05 s, but the computation time is much shorter.

In Fig. 5–7 the temperature distributions after first, second, and fourth freezing are shown. The red dashed line marks the area of tumor infiltration.

Fig. 8 presents a temperature history at the selected points. Two points along the axis were chosen, r = 0 m, z = 0.004 m (blue line), r = 0 m, z = 0.008 m (red line), and one point near the necrosis temperature border, r = 0.008 m, z = 0.008 m (orange line). The temperature history is similar for each freezing.

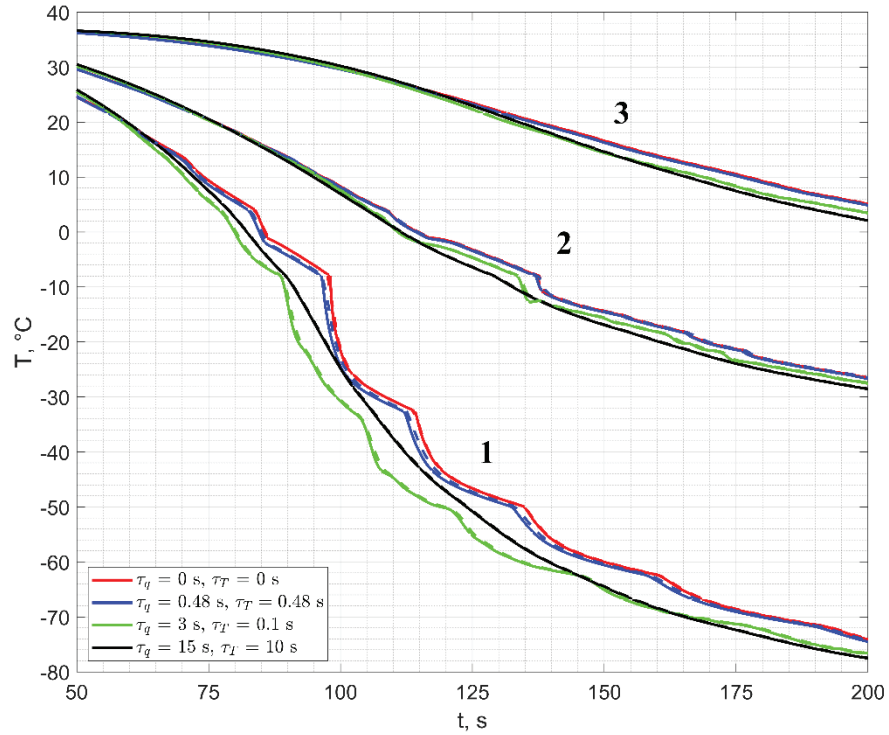

Fig. 3. Temperature history at the points 1 (0, 0.004 m), 2 (0.012 m, 0.004 m), 3 (0.008 m, 0.008 m) from 50 s to 200 s

Rys. 3. Historia temperatury w punktach 1 (0, 0.004 m), 2 (0.012 m, 0.004 m), 3 (0.008 m, 0.008 m) od 50 s do 200 s

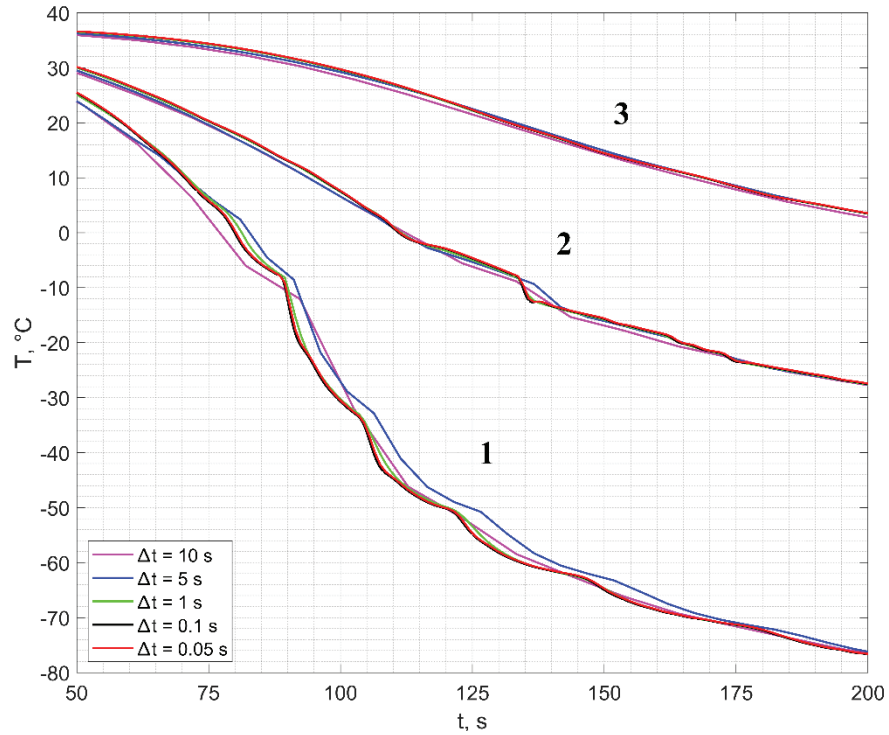

Fig. 4. Temperature history points 1 (0, 0.004 m), 2 (0.012 m, 0.004 m), 3 (0.008 m, 0.008 m) depending on the time step in the implicit scheme for case 3, from 50 s to 200 s

Rys. 4. Krzywe stygnięcia w punktach 1 (0, 0.004 m), 2 (0.012 m, 0.004 m), 3 (0.008 m, 0.008 m) w zależności od kroku czasowego w schemacie niejawnym dla przypadku 3, od 50 s do 200 s

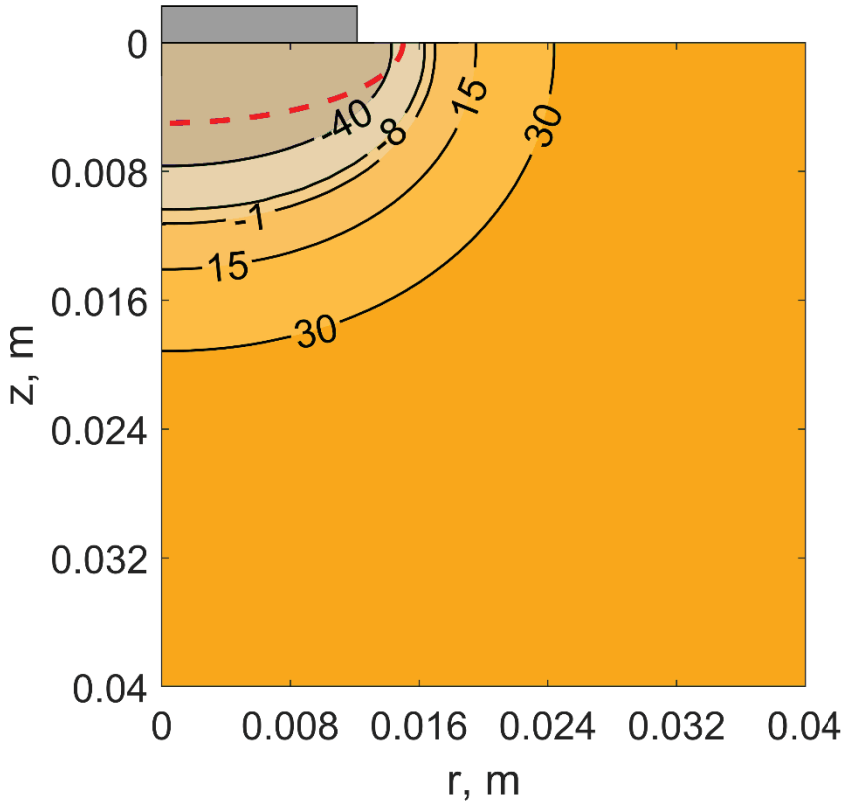

Fig. 5. Temperature distribution after first freezing (t = 6 min 40 s)

Rys. 5. Rozkład temperatur po pierwszym zamrażaniu (t = 6 min 40 s)

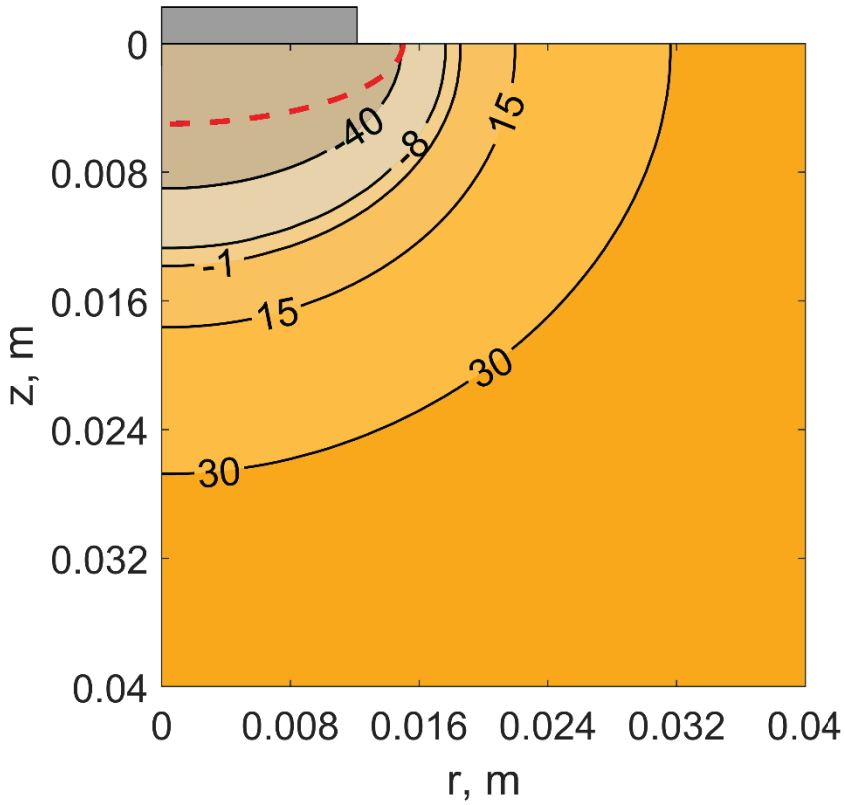

Fig. 6. Temperature distribution after second freezing (t = 52 min 42 s)
Rys. 6. Rozkład temperatur po drugim zamrażaniu (t = 52 min 42 s)

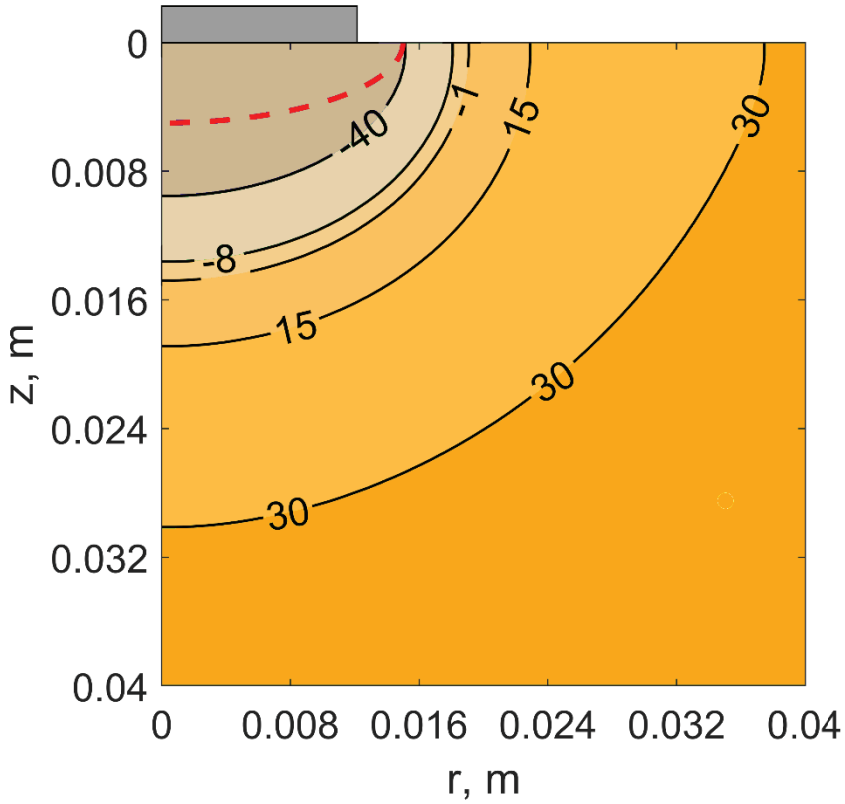

Fig. 7. Temperature distribution after fourth freezing (t = 2 h 24 min 46 s)
Rys. 7. Rozkład temperatur po czwartym zamrażaniu (t = 2 h 24 min 46 s)

After the third and fourth freezing, a slight increase in the frozen subdomain and the necrosis subdomain is observed (Tab. 1).

The numerical analysis carried out shows that for the considered malignant melanoma, a fourth (and possibly a third) freezing during the cryosurgical procedure is not necessary.

Table 1

Frozen and necrosis volume after each freezing

After freezing	Frozen volume (below –8°C) cm^3	Necrosis volume (below –40°C) cm^3	Maximum temperature inside the tumor, °C	Is the entire tumor below the lethal dose?
1	6.17	3.45	–32.1	N
2	8.46	4.29	–42.5	Y
3	9.32	4.59	–45.3	Y
4	9.66	4.71	–46.4	Y

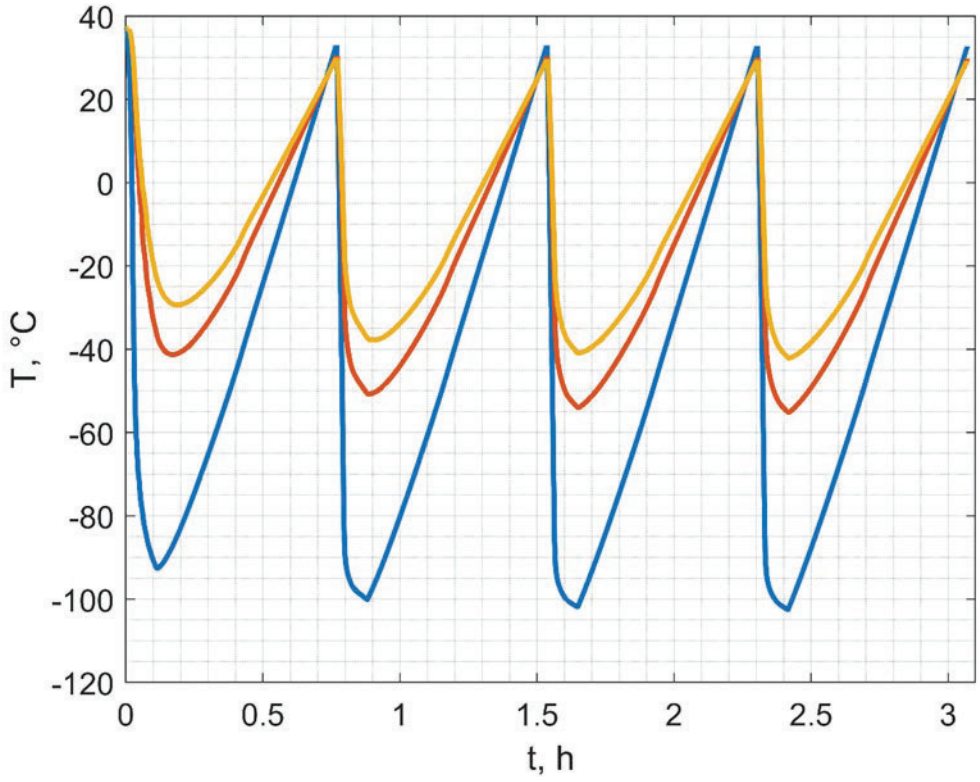

Fig. 8. Temperature history at selected points
Rys. 8. Krzywe stygnięcia/nagrzewania w wybranych punktach

14.5. Conclusions

Numerical modeling of biological tissue freezing can be used as a supporting tool in planning the cryosurgery treatment procedure. Using numerical modeling, one can select the appropriate cryoprobe diameter, tip temperature, freezing and thawing time, cooling rates, number of freezes, predict the size of the necrosis area and determine whether the lethal temperature can reach the entire tumor. The frozen subdomain can also be determined, allowing one to estimate the risk of freezing surrounding healthy tissue.

Bibliography

1. A.A. Gage, J.G. Baust: Mechanisms of tissue injury in cryosurgery, *Cryobiology* (1998) **37(3)**:171–186.
2. B. Rubinsky, C. Lee, J. Bastacky, G. Onik: The process of freezing and the mechanism of damage during hepatic cryosurgery, *Cryobiology* (1990) **27(1)**:85–97.
3. A.M. Granov, D.G. Prokhorov, A.P. Andreev, G.P. Pinaev, G.G. Prokhorov, A.V. Vlasova: Temperature measuring and evaluation of tumor cell viability in different zones of an ice ball. Practical application of in vitro experimental results. In *Basics of Cryosurgery* (Vienna, Austria, 2001) pp. 15–27.
4. J.G. Baust, A.A. Gage, T.E. Bjerklund Johansen, J.M. Baust Mechanisms of cryoablation: clinical consequences on malignant tumors, *Cryobiology* (2014) **68(1)**:1–11.
5. J.G. Baust, A.A. Gage: Progress toward optimization of cryosurgery, *Technology in Cancer Research & Treatment* (2004) **3(2)**:95–101.
6. H.B. Neel, A.S. Ketcham, W.G. Hammond: Requisites for successful cryogenic surgery of cancer, *Archives of Surgery* (1971) **102(1)**:45–48.
7. W.B. Bald, J. Fraser: Cryogenic surgery, *Reports on Progress in Physics* (1982) **45(12)**:1381–1484.
8. A.A. Gage, K. Guest, M. Montes, J.A. Caruana, D.A. Whalen Jr: Effect of varying freezing and thawing rates in experimental cryosurger, *Cryobiology* (1985) **22(2)**: 175–182.

9. E. Mallon, R. Dawber: Cryosurgery in the treatment of basal cell carcinoma: assessment of one and two freeze-thaw cycle schedules, *Dermatologic surgery* (1996) **22(10)**:854–858.
10. D.Y. Tzou: A unified field approach for heat conduction from macro-to micro-scales, *Journal of Heat Transfer* (1995) **117(1)**: 8–16.
11. B. Mochnacki, E. Majchrzak: Numerical model of thermal interactions between cylindrical cryoprobe and biological tissue using the dual-phase lag equation, *International Journal of Heat and Mass Transfer* (2017) **108**:1–10.
12. S. Singh, K. Sushil: Numerical study on triple layer skin tissue freezing using dual phase, *International Journal of Thermal Sciences* (2014) **86**: 12–20.
13. Y. Zhang: Generalized dual-phase lag bioheat equations based on nonequilibrium heat, *International Journal of Heat and Mass Transfer* (2009) **52(21–22)**: 4829–4834.
14. E. Majchrzak, B. Mochnacki: *Metody numeryczne: Podstawy teoretyczne, aspekty praktyczne i algorytmy*, Wydawnictwo Politechniki Śląskiej, Gliwice 1998.
15. E. Majchrzak, B. Mochnacki: Implicit scheme of the finite difference method for 1D dual-phase lag equation, *Journal of Applied Mathematics and Computational Mechanics* (2017) **16(3)**:37–46.
16. E. Majchrzak, B. Mochnacki: Dual-phase lag equation. Stability conditions of a numerical algorithm based on the explicit scheme of the finite difference method, *Journal of Applied Mathematics and Computational Mechanics* (2016) **15(3)**:89–96.
17. A. Breslow: Thickness, cross-sectional areas and depth of invasion in the prognosis of cutaneous melanoma, *Annals of Surgery* (1970) **172(5)**:902–908.
18. H. Drepper, B. Bieß, B. Hofherr, M. Hundeiker, A. Lippold, F. Otto, G. Padberg, A. Peters, H. Wiebelt: The prognosis of patients with stage III melanoma prospective long-term study of 286 patients of the fachklinik hornheide, *Cancer* (1993) **71(4)**:1239–1246.
19. S. Tanaka: Cryosurgery for malignant melanoma. In *Basics of Cryosurgery* (Vienna, Austria, 2001), pp. 289–293.
20. R. Verma, S. Kumar: Computational study on constant and sinusoidal heating of skin tissue using radial basis functions, *Computers in Biology and Medicine* (2020) **121**:103808.

NUMERICAL ANALYSIS OF SKIN TUMOR FREEZING USING DUAL-PHASE LAG MODEL

Abstract

In the paper, the freezing of skin tumors (e.g. malignant melanoma) is considered. The tissue damage mechanism and the freeze-thaw cycle are presented. The thermal interaction between the cryoprobe and tissue is described using a dual-phase lag model (DPLM) in which two phase lags are defined: the relaxation time (associated with the heat flux) and the thermalization time (the temperature gradient lag). Numerical calculations were carried out with the finite difference method (FDM). Implicit and explicit schemes are derived and compared. Finally, numerical modeling of an exemplary cryosurgical procedure is described and analyzed.

Keywords: bioheat transfer, dual phase lag equation, freezing of biological tissue, finite difference method